Improved Stiffness Modeling of Permanent Magnetic Bearings with Relative Permeability Correction

Mante BAEKELAND*, Konstantinos GRYLLIAS*,** and Dirk VANDEPITTE*
* Department of Mechanical Engineering, KU Leuven, Leuven 3001, Belgium
E-mail: mante.baekeland@kuleuven.be
** Flanders Make@KU Leuven, Belgium

Abstract
Analytical stiffness models are most effective in the preliminary design of permanent magnetic bearings (PMBs). While semi-analytical models based on Coulombian and Amperian formulations provide high computational efficiency, they cannot directly account for the finite relative permeability of magnetic materials, potentially leading to an overestimation of bearing stiffness. This paper presents an improved semi-analytical approach that considers the low relative permeability of rare-earth magnets. First, a correction model iteratively estimates the effective magnetization of the magnets, which is then applied as input to idealized semi-analytical stiffness models. Two correction methodologies are proposed and compared: (i) the load line correction method (LLCM), based on magnet demagnetization curves, and (ii) the surface charge correction method (SCCM), based on a surface charge density formulation. These models build on established frameworks and are tailored for PMBs with a focus on reducing the computational cost. The accuracy of the improved semi-analytical models is verified against finite element simulations for axially magnetized radial PMBs. Results show that the LLCM and SCCM improve radial stiffness and axial force estimation. For single-layer radial PMBs, the SCCM achieves lower modeling errors, while the LLCM offers superior computational efficiency. For multi-layer radial PMBs, the LLCM yields lower modeling errors while preserving its computational advantages for the investigated cases. Overall, the improved model offers a computationally efficient and robust design tool, well-suited for preliminary bearing design, particularly in high-precision applications.

Keywords : Permanent Magnetic Bearings, Magnetic Charge Method, Relative Permeability, Electromagnetic, Bearing Stiffness

1. Introduction

Permanent magnet bearings (PMBs) have emerged in a wide range of applications where space efficiency, low maintenance, and minimal heat generation are critical. These bearings are composed of concentric ring magnets, often made from rare-earth materials, arranged in either single-layer or multi-layer (stacked) configurations, with varying polarization directions. Recent advancements in power density and manufacturing (Cui et al., 2022) have enabled the integration of PMBs into small-scale rotary systems. One notable application is their use in magnetic bearing reaction wheels, actuated flywheels used for satellite attitude control, currently under investigation at KU Leuven (Baekeland et al., 2025). In precision systems, accurate tailoring of the stiffness characteristics is essential for achieving the desired rotor dynamic performance.

A common method for evaluating the stiffness characteristics of PMB is magnetostatic finite element analysis (FEA), which allows for the modeling of complex geometries and nonlinear magnetic material behavior (Curti et al., 2015). However, the relatively high computational cost of FEA makes it less practical for preliminary design and iterative optimization processes. To this extent, a wide range of fast (semi-)analytical models have been proposed for modeling PMBs in free space, including the classical surface charge density (Coulombian) and current sheet (Amperian) models (Curti et al., 2015). Due to their mesh-free formulations, these models retain high accuracy even in regions with strong magnetic field gradients, such as near magnet

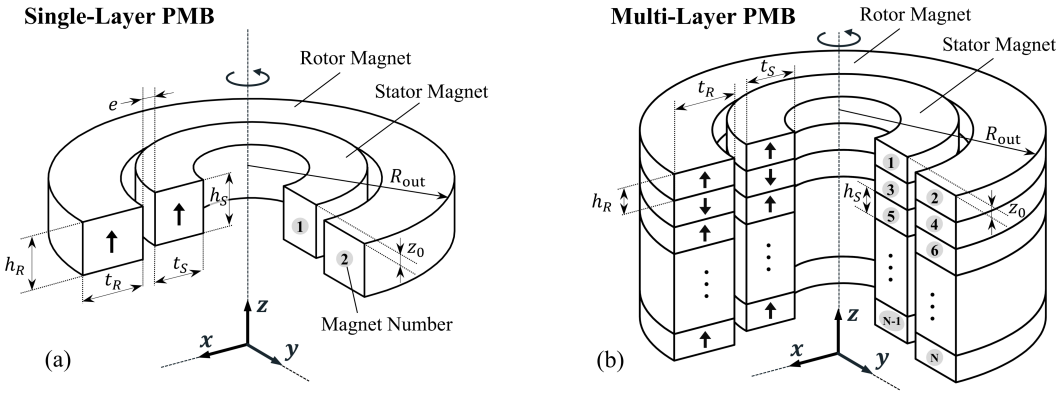

Fig. 1 Cut-through illustration of (a) a single-layer and (b) a multi-layer radial permanent magnetic bearing (PMB) composed of axially magnetized ring magnets, with indicated dimensions.

edges (Kremer et al., 2013). However, the applicability of these models often relies on the assumption that the relative permeability of the permanent magnets is unity ($\mu_r = 1$). As rare-earth magnets (NdFeB and SmCo) typically have a relative permeability in the range of $1.0 - 1.1$ (Kontos et al., 2020), this assumption may lead to a non-negligible modeling error (Van Casteren et al., 2014a). Several improved modeling frameworks have been proposed to address this limitation. Van Casteren et al. (2014a) introduced a general 3D surface charge model that incorporates finite relative permeability for cuboidal magnets, albeit with a high computational cost. A polynomial approximation was proposed in subsequent work to improve efficiency (Van Casteren et al., 2014b). Alternatively, Zhang et al. (2020) proposed a one-dimensional model to estimate the working point and interaction forces between magnets. Despite these advances, much of the existing research remains centered on cuboidal magnets or relies on computationally demanding models, limiting their broader applicability.

This study presents a computationally efficient framework for estimating the stiffness of PMBs that accounts for the non-unity relative permeability of rare-earth magnets. The methodology follows a two-step process. First, two correction strategies are proposed to compute an equivalent magnetization for each magnet that incorporates the effects of relative permeability. These models build upon established improved modeling frameworks and are tailored for PMBs, with an emphasis on reducing computational costs. In the second step, this equivalent magnetization is incorporated into ideal semi-analytical models for predicting bearing stiffness and force characteristics. The proposed correction step remains compatible with a wide range of existing bearing models. The accuracy of the improved model is verified through comparison with FEA results, including an evaluation of both correction methodologies. To demonstrate the applicability of this framework, the study focuses on a classical radial PMB topology composed of axially magnetized ring magnets, examined in both single- and multi-layer arrangements, as shown in Fig. 1. The target application is a compact magnetic suspension system for a flywheel, in which the bearing provides both radial and rotational stabilization (Baekeland et al., 2024). The remainder of the paper is organized as follows: Section 2 presents the mathematical framework and correction methods, while Section 3 covers the verification performed using FEA.

2. Mathematical Framework

The PMB is modeled as a system of N interacting ring magnets with rectangular cross-sections (see Fig. 1). Each magnet i is assumed to be isotropic and homogeneous, characterized by a uniform relative permeability $\mu_{r,i}$. Under this assumption, the magnetization vector $\mathbf{M}_i$ of the magnet is expressed in terms of its residual magnetization $\mathbf{M}_{0,i}$ and magnetic field strength $\mathbf{H}_i$ as:

$$\mathbf{M}_i = \mathbf{M}_{0,i} + (\mu_{r,i} - 1)\, \mathbf{H}_i \tag{1}$$

Alternatively, the magnetization can be formulated via the magnetic flux density $\mathbf{B}_i$ and vacuum permeability μ_0:

$$\mathbf{M}_i = \frac{1}{\mu_{r,i}} \mathbf{M}_{0,i} + \frac{\mu_{r,i} - 1}{\mu_0\, \mu_{r,i}} \mathbf{B}_i \tag{2}$$

For axially magnetized ring magnets, the residual magnetization is given by $\mathbf{M}_{0,i} = \pm B_{\mathrm{rem},i}/\mu_0\ \mathbf{e}_z$, with $B_{\mathrm{rem},i}$ the remanent flux density, and $\mathbf{e}_z$ the unit vector in the axial direction. The sign indicates the direction of magnetization. It is further assumed that no external magnetic field acts on the system. The difficulty lies in a suitable approximation for the second term in Eqs. (1) and (2), which accounts for the influence of non-unity relative permeability and the interaction with other magnets in the system. Instead of solving the non-ideal formulation directly, an equivalent magnetization is derived for further analysis. Two correction methodologies are proposed in this study and adapted for PMBs: (i) the load line correction method (LLCM), which extends the one-dimensional magnetization model of Zhang et al. (2020) by incorporating the demagnetization factor formulation of Beleggia et al. (2009), resulting in a correction approach tailored to PMBs; and (ii) the surface charge correction method (SCCM), which builds on the surface charge density formulation by Van Casteren et al. (2014a, 2014b), adapted to the PMB context and simplified to enhance computational efficiency.

2.1. Load Line Correction Method (LLCM)

The analysis is simplified by considering only the axial component of the magnetization vector, consistent with the magnet's residual magnetization direction. Equation (3) provides a scalar equation for the axial magnetization strength $M_{z,i}$ of magnet i. This expression corresponds to determining the operating point of the magnet using the idealized demagnetization (BH) curves and load lines, as illustrated in Fig. 2a.

$$M_{z,i} = (\mathbf{M}_{0,i} \cdot \mathbf{e_z}) + (\mu_{r,i} - 1) \cdot H_{z,i} \tag{3}$$

$$= (\mathbf{M}_{0,i} \cdot \mathbf{e_z}) + (\mu_{r,i} - 1) \cdot (H_{z,\mathrm{self}} + H_{z,\mathrm{appl}}) \tag{4}$$

The axial magnetic field $H_{z,i}$ is modeled as the superposition of the magnet's self-demagnetization field $H_{z,\mathrm{self}}$ and the applied magnetic field $H_{z,\mathrm{appl}}$ induced by other magnets in the system. The calculation of these terms is outlined in the following steps. First, the self-demagnetization field $H_{z,\mathrm{self}}$ is expressed using the axial demagnetization factor $N_{z,i}$, which defines the slope of the load line (see Fig. 2a):

$$H_{z,\mathrm{self}} = -N_{z,i} M_{z,i} \quad \text{with} \quad N_{z,i} = f\,(R_{\mathrm{in}}/R_{\mathrm{out}},\ h/R_{\mathrm{out}}) \tag{5}$$

Beleggia et al. (2009) derived a semi-analytical expression for $N_{z,i}$ for permanent ring magnets with rectangular cross-sections. The formulation employs complete elliptical integrals, enabling computationally efficient evaluation. As shown in Fig. 2b, the axial demagnetization factor depends solely on the geometry of the magnet, specifically the ratio of the inner to outer radii $R_{\mathrm{in}}/R_{\mathrm{out}}$ and the magnet height-to-outer radius aspect ratio h/R_{out}. Magnets with large diameters and flat profiles exhibit higher demagnetization factors, resulting in more significant reductions in magnetization strength. Notably, for ring magnets with square cross-sections $N_{z,i} \approx 0.5$. Second, in line with the methodology proposed by Zhang et al. (2020), the applied axial magnetic field $H_{z,\mathrm{appl}}$ can be approximated by the volumetric average of the total external magnetic field $H_{z,i}^{\mathrm{ext}}$ over the volume V_i of

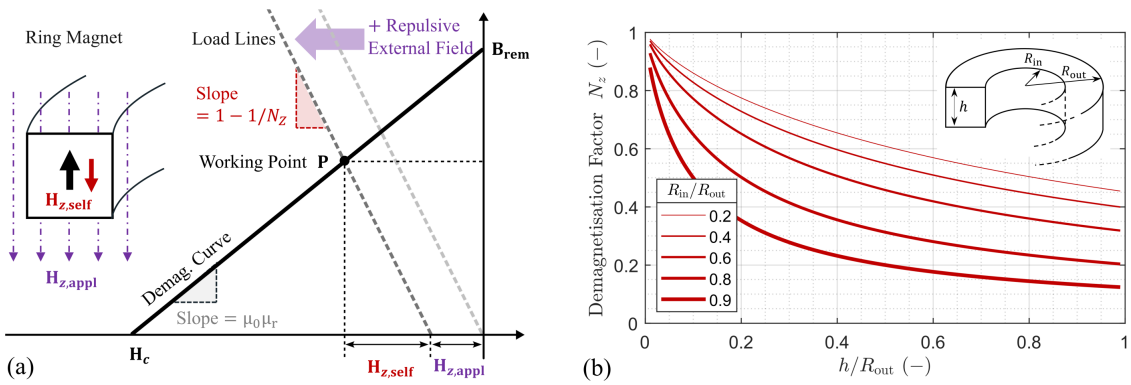

Fig. 2 (a) Illustration of the load line correction method showing the demagnetization curve and load line determining the magnet working point. (b) Axial demagnetization factor $N_z \in [0, 1]$ as a function of the ring magnet's dimension.

magnet i, leading to Eq. (6). The field $H_{z,i}^{\text{ext}}$ results from the superposition of contributions $H_{z,\langle j\rangle\to\langle i\rangle}$ from all other magnets $j \neq i$. Analytical expressions for the magnetic field $H_{z,\langle j\rangle\to\langle i\rangle}$ of an axially magnetized ring magnet are well established in literature (Gallego et al., 2019), using the complete elliptical integral formulation.

$$H_{z,\text{appl}} \approx \overline{H}_{z,\text{appl}} = \frac{1}{V_i}\iiint H_{z,i}^{\text{ext}}\, dV_i = \frac{1}{V_i}\iiint \left(\sum_{j\neq i} H_{z,\langle j\rangle\to\langle i\rangle}\right) dV_i \tag{6}$$

Finally, through the substitution and rearrangement of Eqs. (4)–(6), this work establishes a general expression for the equivalent magnetization. Since the applied magnetic field $\overline{H}_{z,\text{appl}}$ is a function of the magnetization strength of the other magnets, the system is solved iteratively. As an initial estimate (Iter 0), $\overline{H}_{z,\text{appl}}$ is taken to be zero. The resulting expressions are summarized below, with the superscript (n) denoting the iteration step:

$$\text{Iter 0: } M_{z,i}^{(0)} = \frac{\mathbf{M}_{0,i}\cdot\mathbf{e_z}}{1 - N_{z,i} + \mu_{r,i}N_{z,i}} \qquad \text{Iter 1...n: } M_{z,i}^{(n)} = \frac{(\mathbf{M}_{0,i}\cdot\mathbf{e_z}) + (\mu_{r,i}-1)\,\overline{H}_{z,\text{appl}}^{(n-1)}}{1 - N_{z,i} + \mu_{r,i}N_{z,i}} \tag{7}$$

One advantage of this correction approach is that demagnetization curves are commonly provided by magnet suppliers, making it possible to account for non-ideal behavior, including temperature effects and knee points.

2.2. Surface Charge Correction Method (SCCM)

In the classical magnetic charge model, a permanent magnet is represented by fictitious magnetic charges distributed over its boundary surfaces (Curti et al., 2015), as illustrated in Fig. 3. The surface charge density on surface k of ring magnet i is given by:

$$\sigma_{\langle i,k\rangle}(\mathbf{r}) = \mathbf{M}_i \cdot \mathbf{n}_k, \tag{8}$$

where $\mathbf{n}_k$ is the outward-facing unit normal vector of surface k, and $\mathbf{r}$ the position vector. Ring magnets have four surfaces, denoted as $+z$, $-z$, $+r$, and $-r$, according to their surface normals. Van Casteren et al. (2014a) introduced an improved surface charge density model for materials with a constant $\mu_{r,i}$. Starting from Eq. (2) and using a suitable approximation for $\mathbf{B}_i$, following expression was derived, with notation adapted for clarity:

$$\sigma_{\langle i,k\rangle}(\mathbf{r}) = \frac{2}{\mu_{r,i}+1}\left(\mathbf{M}_{0,i}\cdot\mathbf{n}_k\right) + \frac{2(\mu_{r,i}-1)}{\mu_{r,i}+1}\left(\sum_{\langle j,l\rangle\neq\langle i,k\rangle}\mathbf{H}_{\langle j,l\rangle\to\langle i,k\rangle}\cdot\mathbf{n}_k\right) \tag{9}$$

where $\mathbf{H}_{\langle j,l\rangle\to\langle i,k\rangle}$ denotes the field induced by surface l of magnet j on surface k of magnet i. This field is calculated by integrating the contribution of the surface charge density $\sigma_{\langle j,l\rangle}(\mathbf{r}')$ over its surface $dS_{\langle j,l\rangle}$:

$$\mathbf{H}_{\langle j,l\rangle\to\langle i,k\rangle}(\mathbf{r}) = \frac{1}{4\pi}\iint \frac{\sigma_{\langle j,l\rangle}(\mathbf{r}')\left(\mathbf{r}-\mathbf{r}'\right)}{|\mathbf{r}-\mathbf{r}'|^3}\, dS_{\langle j,l\rangle} \tag{10}$$

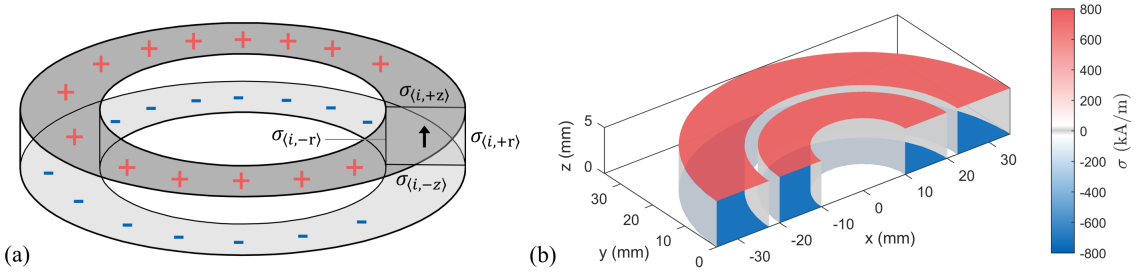

Fig. 3 (a) Illustration of the equivalent surface charge model for an axially magnetized ring magnet. (b) Calculated charge distribution of a single-layer radial PMB with $B_{\text{rem,i}} = 1.25\,\text{T}$, $\mu_{r,i} = 1.05$.

In this work, the proposed model is tailored to the PMB context, with computational efficiency improved through several simplifications. First, only the surface charge densities on the top and bottom faces of the magnets are considered, an assumption justified for low values of $\mu_{r,i}$, as demonstrated in Fig. 3. Second, the magnets are assumed to be radially centered, thereby reducing the analysis from three to two dimensions. Third, for the initial estimation of the surface charge density (Iter 0), the interaction with other magnets is neglected. In summary, the following iterative equations are obtained, where the superscript (n) denotes the iteration step:

$$\begin{aligned}
\text{Iter 0: } \sigma^{(0)}_{\langle i,k\rangle}(r,z) &= \frac{2\mathbf{M}_{0,i}\cdot\mathbf{n}_k}{\mu_{r,i}+1} + \frac{2(\mu_{r,i}-1)}{\mu_{r,i}+1}\left(\sum_{l\neq k} \mathrm{H}_{\langle i,l\rangle\to\langle i,k\rangle}\cdot\mathbf{n}_k\right) && k,l=\{+z,-z\}\\
\text{Iter 1...n: } \sigma^{(n)}_{\langle i,k\rangle}(r,z) &= \frac{2\mathbf{M}_{0,i}\cdot\mathbf{n}_k}{\mu_{r,i}+1} + \frac{2(\mu_{r,i}-1)}{\mu_{r,i}+1}\left(\sum_{\langle j,l\rangle\neq\langle i,k\rangle} \mathrm{H}^{(n-1)}_{\langle j,l\rangle\to\langle i,k\rangle}\cdot\mathbf{n}_k\right) && \begin{matrix} i,j=1,\ldots,N \\ k,l=\{+z,-z\}\end{matrix}
\end{aligned} \tag{11}$$

Finally, rather than evaluating the magnetic interaction force directly from the surface charge distribution, the charge profiles obtained after iteration are used to derive an equivalent magnetization for all ring magnets. This equivalent magnetization strength $M_{z,i}$ is determined as half the difference between the radially weighted average of the surface charge distributions on the top and bottom planes, as given by:

$$M_{z,i} \approx \frac{\overline{\sigma}_{\langle i,+z\rangle} - \overline{\sigma}_{\langle i,-z\rangle}}{2} \quad \text{with} \quad \overline{\sigma}_{\langle i,k\rangle}(z) = \frac{\sum r\cdot\sigma_{\langle i,k\rangle}(r,z)}{\sum r} \tag{12}$$

2.3. Methodology for Stiffness and Force Calculation

The methodology for the computation of the bearing characteristics of PMBs follows a two-step approach. Given the geometry and material properties of the bearing, including the relative permeability, the first step involves the calculation of the equivalent magnetization strength of all ring magnets. This can be achieved iteratively using either the LLCM or the SCCM formulation. Once the equivalent magnetizations are determined, established idealized semi-analytical models are applied to compute bearing stiffness and forces. This study adopts the model proposed by Gallego et al. (2019). Assuming an equal magnetization strength across all magnets, the semi-analytical model shows a quadratic dependence of both stiffness and force on magnetization strength, underscoring the impact of relative permeability corrections, even for values close to unity. The improved semi-analytical model is implemented in MATLAB.

3. Verification with FEA

The accuracy of the proposed correction methodologies is evaluated by comparing the results, on the one hand, with an idealized semi-analytical model assuming $\mu_{r,i} = 1$, and on the other hand, with finite element (FE) simulations performed in ANSYS Maxwell v2022. The study concentrates on radial bearing stiffness and axial forces due to their practical relevance. Both single- and multi-layer radial PMBs are considered. In addition to a general verification approach, a reference bearing is used throughout this analysis, with its dimensions specified in Table 1 and its layout illustrated in Fig. 1. Specifically, the single-layer case consists of $N = 2$ magnets, while the multi-layer case consists of $N = 8$ magnets. In addition to model accuracy, the number of iterations and the computational efficiency of the proposed correction step are also investigated.

Table 1 Geometric and material properties of the reference bearing

Property	Description	Value	Unit
$h_R = h_S$	Axial height of magnet	5.0	mm
t_R	Radial width of rotor magnet	12.5	mm
t_S	Radial width of stator magnet	10.0	mm
R_{out}	Outer radius of bearing	35.0	mm
e	Clearance	2.5	mm
$B_{\text{rem},i}$	Remanent flux density	1.25	T
$\mu_{r,i}$	Relative permeability	1.05	-

3.1. Convergence Rate and Computational Cost

The number of iterations required for the correction step to converge is investigated in Table 2a for a single-layer radial PMB with the dimensions specified in Table 1. Both the LLCM and SCCM converge within two iterations. The computational cost of the correction step is listed in Table 2b. For the single-layer PMB, the computation time is under 10 ms for the LLCM and under 1 s for the SCCM. Computational time scales approximately quadratically with the number of magnets. Even for larger multi-layer PMB configurations, the LLCM remains two orders of magnitude faster than the SCCM, with a computational effort comparable to that required to evaluate stiffness using idealized semi-analytical models (Gallego et al. 2019). In comparison, FE simulations for a single-layer PMB require 5 to 30 minutes, depending on the targeted accuracy and mesh size.

Table 2a Influence of iteration count on equivalent polarisation strength for a single-layer PMB ($N = 2$).

Method	Polarisation	B_{rem}	Iter 0	Iter 1	Iter 2
LLCM	$\mu_0 M_{z,S}$ (T)	1.250 →	1.211	1.204	1.204
	$\mu_0 M_{z,R}$ (T)	1.250 →	1.208	1.206	1.206
SCCM	$\mu_0 M_{z,S}$ (T)	1.250 →	1.206	1.201	1.201
	$\mu_0 M_{z,R}$ (T)	1.250 →	1.204	1.202	1.202

Table 2b Mean computation time for determining the equivalent magnetization of a multi-layer PMB as a function of the number of magnets N, considering 2 iterations (Iter 2), averaged over 10 simulations.

Method	$N = 2$	$N = 4$	$N = 6$	$N = 8$	$N = 10$
LLCM	<10ms	<50ms	0.1s	0.2s	0.5s
SCCM	0.9s	5.3s	12.1s	24.0s	32.5s

3.2. Single-Layer PMB

The initial verification campaign comprises 60 single-layer bearing configurations spanning a broad range of magnet sizes and shapes to explore the full design space, illustrated in Fig. 4. Radial stiffness K_x is computed using the improved semi-analytical model, both with and without the proposed correction procedures. The relative permeability, considered equal for all magnets ($\mu_{r,i} = \mu_r$), is varied from 1.0 to 1.1 in increments of 0.025. Subsequently, the relative error ε_{rel} between the semi-analytical and FE results is computed. Figure 4 shows that the relative error associated with the idealized semi-analytical model increases approximately linearly with μ_r. The correction step significantly improves accuracy. For $\mu_r = 1.1$, the mean relative error decreases from approximately 15.9% to 2.7% using the LLCM, and further to 0.7% with the SCCM. Although the SCCM yields slightly better accuracy than the LLCM, this gain comes at the expense of increased computational cost.

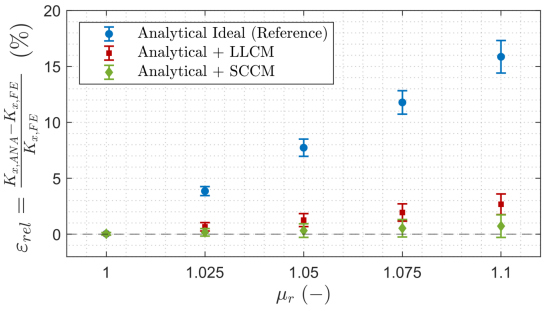

Single-Layer PMB Simulation Cases

Parameter		Value
Bearing Shape	$h_R/t_R = h_S/t_S$	[0.50, 0.75, 1.00, 1.25, 1.50]
Bearing Size	$t_R/e = t_S/e$	[3, 5, 7, 9]
Mean Radius	$R_m = R_{out} - t_R - e/2$	[20, 35, 50] mm
Clearance	e	2 mm
Bearing Offset	z_0	0 mm
Rem. Flux Density	$B_{rem,R} = B_{rem,S}$	1.25 Tesla
Number of Magnets	N	2

Fig. 4 Relative error (mean ± std) in radial stiffness for ideal and corrected semi-analytical (ANA) results compared to finite element (FE) results across 60 axially magnetized single-layer radial PMB configurations (300 simulations total). An overview of the simulation cases is provided.

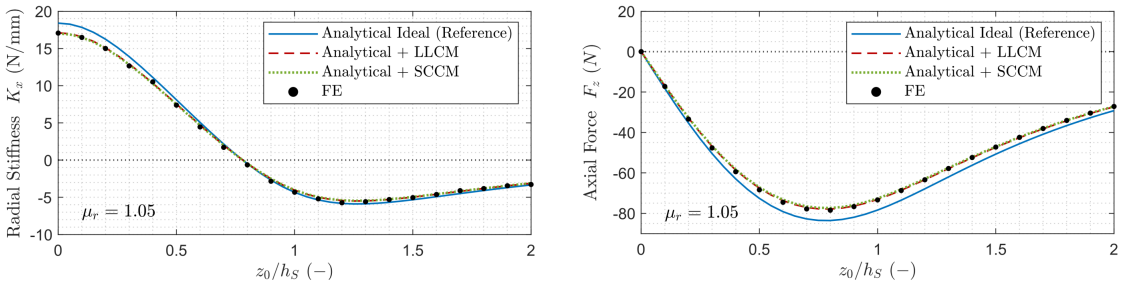

Fig. 5 Radial stiffness and axial forces as functions of non-dimensionalized bearing offset for the single-layer reference PMB, comparing semi-analytical results with FE results.

Additionally, the effect of bearing offset is examined using a reference single-layer PMB, specified in Table 1. Bearing offset is a widely adopted design practice for introducing an axial preload, with one notable application in flywheels, where the preload counterbalances rotor weight and reduces frictional losses in the axial support (Filion et al., 2013). Figure 5 shows radial stiffness and axial force as functions of bearing offset, calculated using the different methodologies. For axial force, the improved semi-analytical model reduces the mean relative error from approximately 6.8% to less than −1.1% for both correction methods. Regarding radial stiffness, the accuracy is significantly improved in the stable region where $K_x > 0$. However, in the quasi-stable and unstable regions where $K_x \leq 0$, the correction models slightly underestimate the radial bearing stiffness. Nevertheless, the practical implication is limited when designing a radially stable PMB.

3.3. Multi-Layer PMB

The radial stiffness is evaluated for 36 multi-layer bearing configurations with variable shapes, sizes, and numbers of magnets using both the ideal and corrected analytical models. Results are verified through comparison with FEA, with μ_r varied between 1.0 and 1.1. Figure 6 shows that the relative error of the ideal model is comparable to that observed for the single-layer PMB cases (Fig. 4). The application of the correction model effectively reduces the relative error, with the LLCM yielding a lower mean error than the SCCM, which tends to underestimate radial stiffness. At $\mu_r = 1.1$, the mean relative error decreases from 17.3% to 0.4% using the LLCM and to −2.3% using the SCCM. Similar trends are observed across different magnet counts, confirming the effectiveness of the LLCM in evaluating the radial stiffness of the multi-layer PMBs at zero bearing offset. Further investigation is required to assess generalization to other bearing configurations and characteristics.

Figure 7 shows the effect of bearing offset for an axially magnetized multi-layer radial PMB ($N = 8$), with dimensions and material properties provided in Table 1. For radial stiffness, the improved model yields a more accurate estimate in the stable region ($K_x > 0$), while in the quasi-stable and unstable region ($K_x \leq 0$), both correction methods slightly underestimate the radial stiffness. These trends align with the results for the single-layer PMB configuration (see Fig. 5). Conversely, for axial force, the correction models consistently provide an underestimate compared to the FE results, with a mean relative error below 4.8% for both correction approaches. In terms of computational cost, the ideal analytical model requires approximately 0.3 s, while employing the LLCM and SCCM increases the total average computation time to 0.6 s and 24.3 s, respectively.

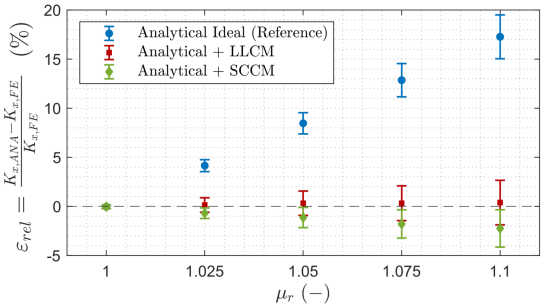

Multi-Layer PMB Simulation Cases

Parameter		Value
Bearing Shape	$h_R/t_R = h_S/t_S$	[0.50, 0.75, 1.00]
Bearing Size	$t_R/e = t_S/e$	[3, 5]
Mean Radius	$R_m = R_{out} - t_R - e/2$	[20, 35] mm
Clearance	e	2 mm
Bearing Offset	z_0	0 mm
Rem. Flux Density	$B_{rem,i}$	1.25 Tesla
Number of Magnets	N	[6, 8, 10] magnets

Fig. 6 Relative error (mean ± std) in radial stiffness for ideal and corrected semi-analytical (ANA) results compared to finite element (FE) results across 36 axially magnetized multi-layer radial PMB configurations (180 simulations). An overview of the simulation cases is provided.

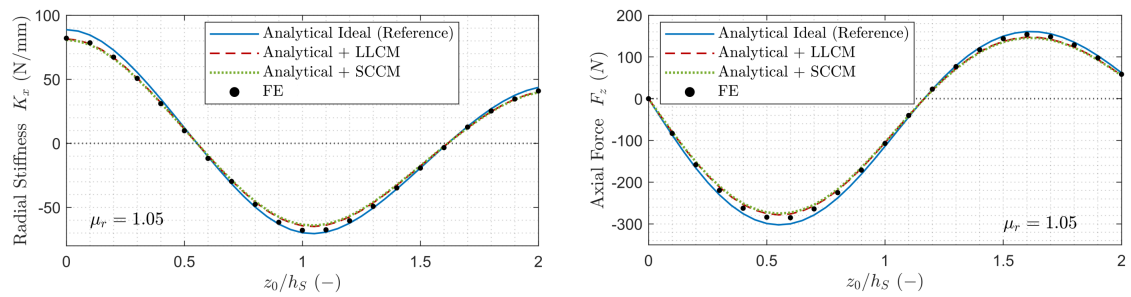

Fig. 7 Radial stiffness and axial forces as functions of non-dimensionalized bearing offset for the multi-layer reference PMB, comparing semi-analytical results with FE results.

4. Conclusion

This paper presents an improved semi-analytical model for calculating the stiffness of radial PMBs, accounting for the low relative permeability values typical of rare-earth magnets. The study addresses both single- and multi-layer radial PMBs composed of axially magnetized ring magnets. The proposed methodology employs a two-step correction procedure, where an equivalent magnetization strength is first computed for all magnets. Verification against FEA results demonstrates that both the load line correction method (LLCM) and the surface charge correction method (SCCM) substantially reduce modeling errors in radial stiffness and axial force predictions. For single-layer PMBs with zero bearing offset, the SCCM achieves lower modeling errors in radial stiffness, whereas the LLCM offers superior computational speed of up to two orders of magnitude. In the multi-layer PMB cases, the LLCM provides the most accurate approximation, with a mean relative error below 1%. However, when bearing offset is introduced, both correction methods tend to slightly underestimate bearing stiffness in the region where $K_x \leq 0$, for both single- and multi-layer configurations.

Overall, the improved semi-analytical model is computationally efficient, particularly when employing the LLCM. Combined with the LLCM's demonstrated accuracy for axially magnetized radial multi-layer PMBs, this framework holds promise for further optimization of bearing designs. A notable limitation is that the proposed model is only valid for low relative permeability values and therefore cannot be used to model steel. Consequently, more computationally demanding analytical models or FE simulations remain necessary for such cases. Finally, although this study focused on the radial stiffness and axial force of radial PMBs, the proposed framework is readily extendable to a broader range of PMB configurations and other bearing characteristics.

5. Acknowledgments

The Research Foundation - Flanders (FWO) is gratefully acknowledged for its support through research grant number 1SH5924N. The authors would like to thank ESA/ESTEC for their support and funding under ESA Contract No. 4000136555/21/NL/CLP.

References

Baekeland, M., Cuypers, C., Seiler, R., et al., Modelling and tuning of a permanent magnetic suspension system for low-vibration flywheels, Proceedings of the 2024 International Conference on Noise and Vibration Engineering (ISMA), Leuven, Belgium (2024).

Baekeland, M., Lanting, J., Cuypers, C., et al., Design of a compact passive magnetic bearing support for reaction wheels to minimize vibration emission, Proceedings of the 4S Symposium, Palma de Mallorca, Spain (2025). DOI:10.1117/12.3061929.

Beleggia, M., Vokoun, D. and De Graef, M., Demagnetization factors for cylindrical shells and related shapes, Journal of Magnetism and Magnetic Materials, Vol.321, No.9 (2009), pp.1306–1315. DOI:10.1016/j.jmmm.2008.11.046.

Cui, J., Ormerod, J., Parker, D., Ott, R., Palasyuk, A., et al., Manufacturing processes for permanent magnets: Part I—sintering and casting, JOM, Vol.74, No.4 (2022), pp.1279–1295. DOI:10.1007/s11837-022-05156-9.

Curti, M., Paulides, J. J. H. and Lomonova, E. A., An overview of analytical methods for magnetic field computation, Tenth International Conference on Ecological Vehicles and Renewable Energies (EVER) (2015). DOI:10.1109/EVER.2015.7112938.

Filion, G., Ruel, J. and Dubois, M. R., Reduced-friction passive magnetic bearing: Innovative design and novel characterization technique, Machines, Vol.1, No.3 (2013), pp.98–115. DOI:10.3390/machines1030098.

Gallego, G. B., Rossini, L., Achtnich, T., et al., Force and torque model of ironless passive magnetic bearing structures, Proceedings of the 2019 IEEE International Electric Machines and Drives Conference (IEMDC), San Diego, USA (2019), pp.507–514. DOI:10.1109/IEMDC.2019.8785411.

Kontos, S., Ibrayeva, A., Leijon, J., et al., An overview of MnAl permanent magnets with a study on their potential in electrical machines, Energies, Vol.13, No.21 (2020), p.5549. DOI:10.3390/en13215549.

Kremers, M. F. J., Paulides, J. J. H., Ilhan, E., et al., Relative permeability in a 3D analytical surface

charge model of permanent magnets, IEEE Transactions on Magnetics, Vol.49, No.5 (2013), pp.2299–2302. DOI:10.1109/TMAG.2013.2239976.

Van Casteren, D. T. E. H., Paulides, J. J. H. and Lomonova, E. A., 3-D numerical surface charge model including relative permeability: The general theory, IEEE Transactions on Magnetics, Vol.50, No.11 (2014a), pp.1–4. DOI:10.1109/TMAG.2014.2320194.

Van Casteren, D. T. E. H., Paulides, J. J. H. and Lomonova, E. A., 3-D Semianalytical Surface Charge Model Including Relative Permeability Using Polynomial Approximation, IEEE Transactions on Magnetics, Vol.50, No.11 (2014b), pp.1–4. DOI:10.1109/TMAG.2014.2331984.

Zhang, H., Kou, B. and Zhou, L., An improved surface charge model for the static force calculation among the permanent magnets in magnetic bearings or magnetic springs, IEEE Transactions on Magnetics, Vol.57, No.2 (2020). DOI:10.1109/TMAG.2020.3005245.